Journal of the European Ceramic Society xxx (2016) xxx–xxx

Contents lists available at www.sciencedirect.com

Journal of the European Ceramic Society

journal homepage: www.elsevier.com/locate/jeurceramsoc

Grain-size/(t'' or c)-phase relationship in dense ZrO_2 ceramics

I.O. Fábregas[a,b,*], M. Reinoso[b,c,d], E. Otal[a,b,e], M. Kim[a,b,e]

[a] Division of Porous Materials, UNIDEF-CONICET-CITEDEF, S.J.B. de La Salle 4397, B1603ALO Villa Martelli, Buenos Aires, Argentina
[b] CONICET, Godoy Cruz 2290, C1425FQB CABA, Argentina
[c] Departamento de Física Experimental, GIyA Comisión Nacional de Energía Atómica, Avda. General Paz 1499, 1650 San Martín, Buenos Aires, Argentina
[d] Escuela de Ciencia y Tecnología, Universidad Nacional de San Martín, Martín de Irigoyen 3100, 1650 San Martín, Buenos Aires, Argentina
[e] Laboratory for Materials Science and Technology, FRSC-UTN, Av. Inmigrantes 555, Río Gallegos 9400, Argentina

ARTICLE INFO

Article history:
Received 28 November 2015
Received in revised form 25 January 2016
Accepted 29 January 2016
Available online xxx

Keywords:
Ceramics
Sintering
Crystal structure
Electrochemical impedance spectroscopy
Raman spectroscopy

ABSTRACT

Zirconia-based materials are widely investigated and used as electrolytes in solid-oxide fuel cells, oxygen sensors and electrochemical devices. These materials present polymorphism, which has a critical effect on their technologically important properties. The polymorphism is influenced by, among other factors, aliovalent dopant nature and content, grain size and interfacial energy.

In this work, we investigated the crystal structure of ZrO_2–12 mol% CaO and –9 mol% Y_2O_3 dense ceramics as a function of grain size. We found that the samples undergo a phase transition from the t'' form of the tetragonal phase to the cubic phase with an increase in grain size. This transition is directly detected by Raman spectroscopy and further evidence is given by a change in the activation energy for bulk ionic conduction. The transition occurs at an average grain size greater than 500 nm for both systems.

1. Introduction

Zirconia-based ceramics are intensively investigated and widely used as electrolytes in solid-oxide fuel cells [1], oxygen sensors [2,3], electrochemical devices [4], etc., because they present excellent electrical and mechanical properties, stability in reducing or oxidizing environments and limited or null interdiffusion with typical electrode materials [5–8].

Several authors studied the ZrO_2 equilibrium phase diagram alloyed with diverse oxides. However, there is no final consensus, mainly because it is difficult to differentiate the metastable from the stable phases and also because it is very difficult to reach equilibrium conditions with thermal treatments below 1200 °C [9].

As shown in the phase diagram (Fig. 1), the tetragonal phase is stable only at high temperature. However, in solid solutions with aliovalent oxides such as Y_2O_3, CaO, MgO, etc. or CeO_2, it can be retained at room temperature in a metastable state for nanocrystalline powders and fine-grained sintered ceramics [10–16].

The tetragonal phase presents two additional forms, known as t' and t'', with increasing dopant content; all three tetragonal forms belong to the $P4_2/nmc$ space group. The stable form of the tetragonal phase is called the t-form, which is restricted to the solubility limit predicted by the equilibrium phase diagram and has an axial ratio, c/a, higher than 1 (considering the a lattice constant as in a pseudo fluorite cell, $a_{tetragonal} \times \sqrt{2} = a_{cubic}$). The t'-form, also with $c/a > 1$, has a wider solubility range, but it is thermodynamically unstable; the stable state in this compositional range is a mixture of the t-form and the cubic phase. The t''-form has a $c/a = 1$; it exhibits a fluorite cationic sublattice, but the oxygen atoms are displaced along the c axis from their ideal sites of the cubic phase (8c sites of the $Fm\bar{3}m$ space group). At higher dopant content, a cubic phase of fluorite-like structure is retained [10–16].

Yashima et al. have studied the diffusionless phase transformations leading to the retention of metastable phases at room temperature in doped ZrO_2 systems. These authors were able to obtain compositionally homogeneous solid solutions presenting the cubic or tetragonal structure by melting the precursor oxides followed by quenching. Diffusionless transformations between the t'–t''-cubic phases are usually presented as a T_0 line in a stable-metastable phase diagram (see Fig. 1).

Some properties of zirconia based materials depend on its grain size. Vickers micro-hardness increases with a decreasing grain size. Fracture toughness and the monoclinic martensitic transformation start temperature both increases with grain size (for sizes smaller than 2 μm), for doped zirconia pellets or films [17–19]. Pure and doped zirconia powders present phase transitions with decreasing grain size and/or changes in interfacial energy [20–22]. The bulk

* Corresponding author at: Division of Porous Materials, UNIDEF-CONICET-CITEDEF, S.J.B. de La Salle 4397, B1603ALO Villa Martelli, Buenos Aires, Argentina.
E-mail addresses: Ismaelfabregas@gmail.com, ifabregas@citedef.gob.ar (I.O. Fábregas).

http://dx.doi.org/10.1016/j.jeurceramsoc.2016.01.048
0955-2219/

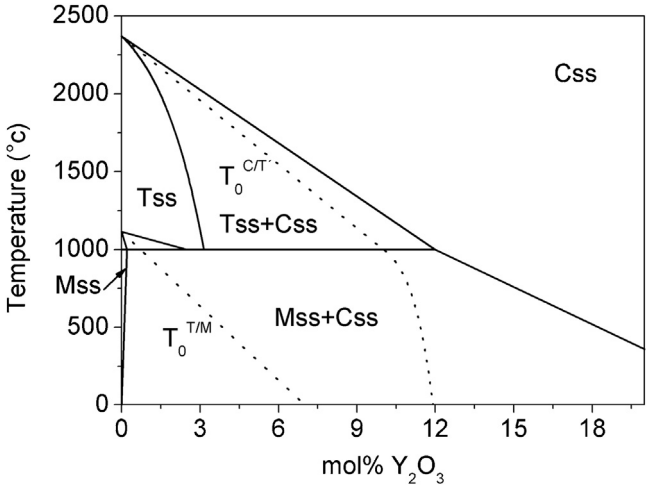

Fig. 1. Stable–metastable phase diagram for the ZrO_2–Y_2O_3 system. Adapted from Ref. [9]. Css: cubic. Tss: tetragonal. Mss: monoclinic. T_0: lines for diffusionless transformation.

ionic conductivity slightly improves with a decreasing grain size in ceramic pellets, also [23–25]. Therefore, it is of interest to know the phase/size (crystallite or grain) relationship. It may even be useful to clarify certain aspects of the conductivity of thin films, where contradictory results were found (whether they are better conductors than bulk ceramics [26,27]).

In this work we studied the crystal structure of dense ZrO_2–12 mol% CaO and ~9 mol% Y_2O_3 ceramics as a function of grain size by X-ray diffraction and Raman spectroscopy. These compositions were chosen because they present the highest conductivity for each system and are one of the most used in technological applications (e.g., electrolytes in solid oxide fuel cells). We used X-ray diffraction to identify the pellets phase and detect any degradation or mixture of phases. Following the intensity of the 470 cm^{-1} band in the Raman spectra allowed us to establish the t''-form/cubic transition as a function of grain size for dense ceramics for both systems. This limit resulted between 500 and 790 nm for ZrO_2–12 mol% CaO and between 500 and 670 nm for ZrO_2–9 mol% Y_2O_3. Additional evidence of this transition is supported by the change in the activation energy (Ea) for bulk ionic conduction, calculated from electrochemical impedance spectroscopy (EIS) measurements.

2. Experimental procedure

Ceramic powders were synthesized by a stoichiometric gel-combustion route explained elsewhere [28]. High purity $ZrO(NO_3)_2{\cdot}6H_2O$ (Sigma–Aldrich, 99.99%), $Y(NO_3)_3{\cdot}6H_2O$ (Sigma–Aldrich, 99.99%) or $Ca(NO_3)_2{\cdot}4H_2O$ (Sigma–Aldrich, 99.99%), were used.

Ceramic pellets were prepared by uniaxial pressing, using a 10 mm diameter die with faces polished to a mirror finish. Typically, 600 MPa of pressure was applied to the powders with a pressureless sintering program of 5 °C min^{-1} heating and cooling rate and a 2 h soak at peak temperature to obtain the pellets. Occasionally, some samples required higher pressure (1290 MPa) or faster heating and cooling rates (400 °C min^{-1}) to obtain dense pellets with a small grain size and t''/c phases. Table 1 summarizes the different samples used in this study and the conditions to obtain them.

When we are not referring to a particular sample but to a series of them, we will use the following convention: Z (for ZrO_2)-composition-dopant. According to this nomenclature the ZrO_2–12 mol% CaO series becomes Z12C.

P-XRD was performed in a Philips PW 3710 laboratory diffractometer, equipped with a graphite monochromator, operated at 40 kV and 30 mA and using Co-Kα radiation. The 2θ = 30–95° range was measured for all samples with a 0.05° step and 180 s/step. The 84–93° range (around the 004 reflection) for all samples and the 30–95° range for Z12C-1220 and Z9Y-1220 samples were measured with a 0.02° step and 500 s/step. Rietveld refinement was performed using a Pseudo-Voigt with the Finger-Cox-Jephcoat asymmetry correction with the GSAS [29]/EXPGUI [30] code. The density of the pellets, previously sanded to eliminate rough edges, was calculated from their mass and geometric volume. The mass was measured with an analytical scale and the volume was determined by measuring its diameter and thickness with a calliper.

Depolarized Raman spectra were taken using a Horiba Jobin-Yvon LabRaman HR spectrometer with a laser source operating at 514 nm (Ar excitation line, spot diameter of 5 μm) with a spectral resolution of 2.5 cm^{-1}. The power was adjusted to minimize heating at the spot. The dispersed beam was analysed in a 180° geometry. 10 scans with a 10s integration time were taken for each sample and averaged.

The microstructure of the ceramic pellets was studied by scanning electron microscopy (SEM), using a Philips 515 or a FESEM DSM 982 Gemini scanning electron microscopes. The pellets were previously sputtered with gold. The average grain size was calculated by measuring the area of at least 200 grains for each sample and fitting $D_g/\langle D_g\rangle$ with the Louat distribution, where $D_g = 2 \times \sqrt{(\text{grain area}/\pi)}$ [31–33].

Electrochemical impedance spectroscopy was conducted in air between 1 MHz and 0.1 Hz with a Princeton Applied Research 273A potenciostat/galvanostat, with an attached frequency response analyser (SI1255). The current collectors were made from silver paint. The paint was left to dry at room temperature and then fired, in air, at 600 °C for an hour, with a 10 °C min^{-1} heating and cooling rate. The spectra were taken between 200 and 850 °C and normalized by their corresponding pellets macroscopic dimensions and density. EIS fittings were performed with the Zview software (version 2.9c, Scribner associates), using a $(RQ)_b(RQ)_{gb}$ equivalent circuit, one RQ for the bulk and another for the grain boundary.

3. Results and discussion

3.1. Microstructural characterization

Table 2 reports the average grain size (D_g) and the relative density, as a percentage of the theoretic one, while Fig. 2 shows the microstructure and the grain size distribution. All the samples showed a different degree of porosity, in accordance with their density. As reported in Ref. [20], phase transitions can be influenced by the interfacial energy, but as shown in Fig. 2, most of the grains had an excellent contact with each other and a high coordination number; the interfacial energy, therefore, should have a similar effect for all the samples.

3.2. Structural characterization

Although the powders used in this work are compositionally homogenous and known to support high temperatures (>1400 °C) without degradation [25,47], concerns about the phase purity of these samples may arise because of the sintering treatment and the lack of a distinctive signal for identifying the presence of the cubic phase.

According to the phase diagram, if there is degradation towards the thermodynamically stable state, two phases should appear: a lightly doped tetragonal phase ($c/a > 1$) and a highly doped cubic one. An analysis of the tetragonal and cubic ZrO_2 phases shows

Please cite this article in press as: I.O. Fábregas, et al., Grain-size/(t'' or c)-phase relationship in dense ZrO_2 ceramics, *J Eur Ceram Soc* (2016), http://dx.doi.org/10.1016/j.jeurceramsoc.2016.01.048

Table 1
Different ZrO_2–Y_2O_3 and ZrO_2–CaO pellets used and conditions to prepare them. Soak temp.: sintering temperature and soak time.

Composition (mol%)	Code	Pressure (MPa)	Rate (°C min^{-1})	Soak temp. (°C) [time]
ZrO_2–2.8% Y_2O_3	Z3Y	600	5	1600 [2 h]
ZrO_2–9% Y_2O_3	Z9Y-1220	1290	5	1220 [1 h]
ZrO_2–9% Y_2O_3	Z9Y-1250	1290	5	1250 [1 h]
ZrO_2–9% Y_2O_3	Z9Y-1290	1290	5	1290 [1 h]
ZrO_2–9% Y_2O_3	Z9Y-1350	600	5	1350 [2 h]
ZrO_2–9% Y_2O_3	Z9Y-1600	600	5	1600 [2 h]
ZrO_2–6% CaO	Z6C	600	400	1350 [7 min]
ZrO_2–12% CaO	Z12C-1220	1290	5	1220 [1 h]
ZrO_2–12% CaO	Z12C-1290	1290	5	1290 [1 h]
ZrO_2–12% CaO	Z12C-1320	1290	5	1320 [1 h]
ZrO_2–12% CaO	Z12C-1350	600	5	1350 [2 h]
ZrO_2–12% CaO	Z12C-1600	600	5	1600 [2 h]

Table 2
Properties of investigated samples and literature survey of Ea. Composition: ceramic composition. D_g: average grain size. Ea: activation energy for bulk ionic conduction. Phase: crystallographic phase, when reported. δ_{theo}%: density as a percentage of the theoretic one. Soak temp.: sintering temperature and soak time. All Ea were calculated from data taken below 500 °C.

Composition	Ceramic D_g (um)	Ea (eV)	Phase	Density (% δ_{theo})	Soak temp. (°C) [time]	Ref.
Z3Y	0.08–0.16	~0.94	*t*	66–100	1050–1200 [<1 h]	[34]
Z3Y	0.05	0.84	*t*	93–96	1000 vacuum [1 h] + O_2 anneal	[35]
Z3Y	0.12	~0.85	97% *t*	97	1150 [2 h]	[36]
Z3Y	0.4	0.92	*t*	Dense	1400 [2 h]	[37]
Z3Y	0.6	0.91 (1)	*t*	94 (2)	1600 [2 h]	This work
Z3Y	0.56–0.69	0.92–0.93	n/a	>99	1500 [4 h]	[38]
Z3Y	0.12–13.3	0.84–0.85	n/a	94–99.9	1175–1600 [2–10 h]	[39]
Z3Y	1.9	0.85	*t*	Dense	1500 [4 h]	[40]
Z8Y	n/a	0.71[a]	*t*″/cubic	n/a	1650 [4 h]	[41]
Z8Y	0.031–0.351	0.96	n/a	93–98	1100–1200 [1 h] (HUP)	[23]
Z8Y	0.01–0.061	~0.93[b]	*t*″/cubic	38–87	800–1050 [1 h]	[42]
Z9Y	0.23	0.94 (2)	*t*″	83 (2)	1220 [1 h]	This work
Z9Y	0.50	0.95 (2)	*t*″	87 (2)	1250 [1 h]	This work
Z9Y	0.67	1.15 (3)	Cubic	90 (2)	1290 [1 h]	This work
Z9Y	0.86	1.14 (2)	Cubic	92 (2)	1350 [2 h]	This work
Z8Y	2.4	1.07	*t*″/cubic	n/a	1400 [6 h]	[24]
Z9Y	3	1.15 (2)	Cubic	93 (2)	1600 [2 h]	This work
Z8Y	3.1–13.9	1.08–1.13	n/a	92.8–99.2	1500 [4 h]	[38]
Z8Y	16	1.05	Cubic	dense	1700 [1 h]	[40]
Z8Y	n/a	~1.15	*t*″/cubic	n/a	1300–1500 [2 h]	[43]
Z8Y	n/a	~1.16	*t*″/cubic	95	1500 [24 h]	[44]
Z10Y	n/a	~1.22	Cubic	n/a	1300–1500 [2 h]	[43]
Z5C	>1	~1.1[b]	Cubic	93	1600 [3 h]	[45]
Z6C	0.65	1.08 (2)	*t*	93 (2)	1350 [7 min]	This work
Z12C	0.35	1.07 (3)	*t*″	75 (2)	1220 [1 h]	This work
Z12C	0.50	1.09 (2)	*t*″	79 (2)	1290 [1 h]	This work
Z12C	0.79	1.27 (2)	Cubic	83 (2)	1320 [1 h]	This work
Z12C	1	1.26 (3)	Cubic	92 (2)	1350 [2 h]	This work
Z12C	1.8	1.28 (2)	Cubic	97 (2)	1600 [2 h]	This work
Z12C	n/a	~1.42	*t*″/cubic	n/a	1300–1500 [2 h]	[43]
Z12C	n/a	1.20	Cubic	n/a	1650 [4 h]	[41]
Z15C	2.7	1.32	Cubic	94	1400 [6 h]	[24]
Z12–19C	22–55	1.13–1.29	*t*″/cubic	56–90	>1550 [>3 h]	[46]

[a] Not commented on its reference, see Section 3.3.
[b] Not reported, calculated from figures. HUP: hot uniaxial pressing.

that satellite peaks belonging to the tetragonal phase should appear before and after the 200, 311, 400, and 420 *t*″/cubic reflections in the XRD pattern. The inset in Fig. 3 shows the region corresponding to the (400) c reflections for the Z12C samples, it is also in this range where (400) t, (004) t should appear; the insert's scale is logarithmic to highlight the eventual presence of low intensity peaks. Clearly, no extra peaks are present (the only other peak, at ~88.5°, is due to the Kα_2). No satellite peaks around the 111 reflection, where the most intense peaks of the monoclinic phase appear, were detected for any of the samples, either.

Another possible concern is related to the slow cooling after sintering. Krogstad et al. [48] found that this treatment could yield a phase with no resolvable tetragonality in the Rietveld refinement for tetragonal samples. But they also stated that, even in slow cooled samples, there was always some asymmetry in the peaks, showing the presence of the (400)t and (004)t reflections. A careful analysis of the (400) reflection profile for our samples provided no evidence of this (see Fig. 3).

Finally, the samples identified as *t*″ might actually be a mixture of *t*″ and cubic phases as there is no distinct Raman mode for the cubic phase. Rietveld refinement was performed for the samples sintered at 1220 °C. A good fit was achieved with one phase (see Table 3 and Fig. 4). Attempts to add an extra phase resulted in divergent refinements or a fraction of less than 0.1% for the second phase; fits with the $P4_2/nmc$ space group resulted in a *c*/*a* indistinguishable from 1 within the error bars.

We thus conclude that the samples used in this study are monophasic. A similar analysis conducted for the Z9Y samples provided the same results.

Please cite this article in press as: I.O. Fábregas, et al., Grain-size/(*t*″ or *c*)-phase relationship in dense ZrO_2 ceramics, *J Eur Ceram Soc* (2016), http://dx.doi.org/10.1016/j.jeurceramsoc.2016.01.048

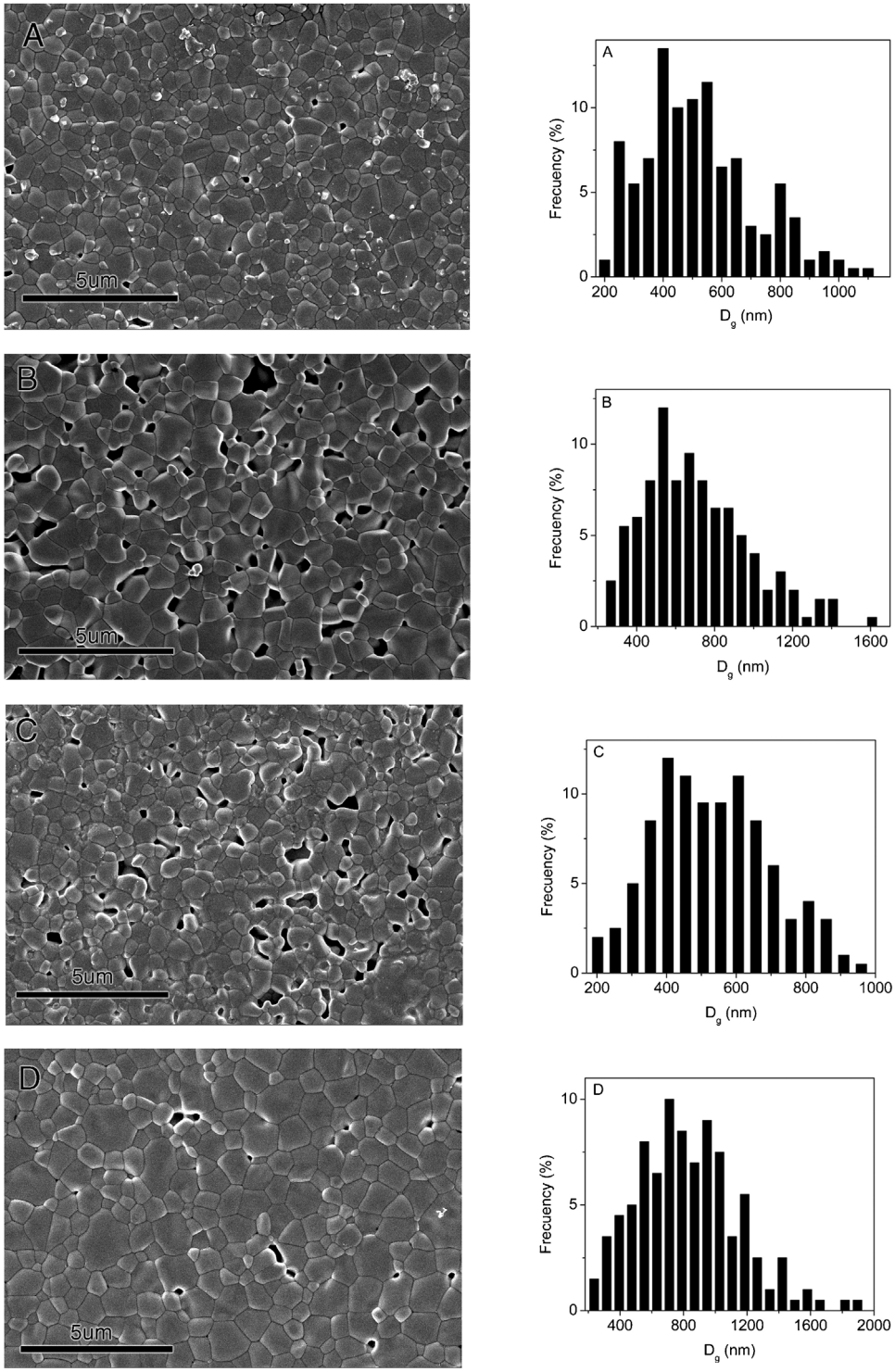

Fig. 2. Micrographs (left) and grain size distribution (right) for the ceramic pellets. (a) Z9Y-1250. (b) Z9Y-1290. (c) Z12C-1290. (d) Z12C-1320.

Table 3
Refined lattice and goodness-of-fit parameters for the Z12C-1220 sample.

	Sample	a (Å)	c (Å)	c/a	Rwp	Rp
$Fm\bar{3}m$	Z12C-1220	5.1292 (5)	–	–	0.0705	0.0486
$P4_2/nmc$	Z12C-1220	3.6277 (4)	5.1305 (2)	1.00003 (11)	0.0857	0.0581

Only one lattice constant is detected (see Table 3 and Fig. 3) for all samples; therefore they presented a fluorite cationic substructure. To determine if they have the t''-form of the tetragonal phase or the cubic phase (both structures have $c/a = 1$), we have to look for

Please cite this article in press as: I.O. Fábregas, et al., Grain-size/(t'' or c)-phase relationship in dense ZrO_2 ceramics, *J Eur Ceram Soc* (2016), http://dx.doi.org/10.1016/j.jeurceramsoc.2016.01.048

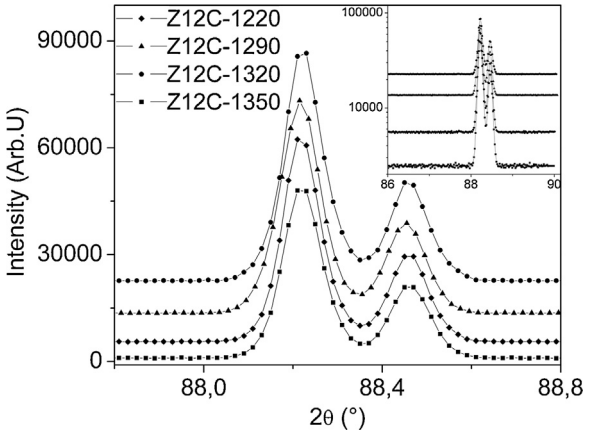

Fig. 3. Z12C sample series X-ray diffraction data corresponding to the (400) c reflection (the presence of two peaks is due to the Co $K\alpha_1$ and $K\alpha_2$ lines). The broader range and logarithmic scale in the inset highlights the absence of tetragonal reflections. This is the range where the (400) t and (004) t reflections should appear if the tetragonal phase were present. The vertical scale is shifted for clarity.

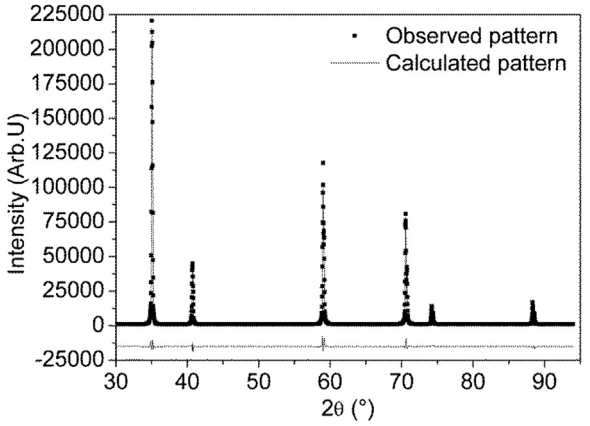

Fig. 4. Diffraction profile for Z12C-1220, with its corresponding calculated profile. The difference between the observed and calculated patterns is shown below.

weak reflections related to the displacement of the oxygen atoms. As the oxygen is a light atom, its reflections are difficult to detect with laboratory XRD.

Raman spectroscopy was used to determine the oxygen displacement; this technique easily distinguishes the t''-form from the cubic phase. Fig. 5 plots the Raman spectra for the Z12C sample series. Six Raman-active modes at approximately 150, 260, 320, 470, 600 and 640 cm^{-1} are detected. All of them are assigned to the tetragonal phase (one A1g, three Eg and two B1g modes), and their positions coincide well with those reported by Yashima et al. [49,50] and our own studies in nano-sized powders [15]. As established by Yashima et al., the occurrence of the 470 cm^{-1} band can be used to monitor the presence of the tetragonal phase [49,50]. With increasing sintering temperature this band monotonically losses intensity and disappears for samples treated at temperatures higher than 1320 °C. This change is indicative of a transition from tetragonal to cubic symmetry [15,49,50].

Similar results were obtained for the Z9Y sample series; in this case the 470 cm^{-1} band disappears for samples treated at temperatures higher than 1290 °C (data not shown).

Consequently, the Raman and XRD studies show that the Z12C-1220 and Z12C-1290 presented the t'' form of the tetragonal phase while the Z12C-1320 and Z12C-1350 samples presented the cubic one. These samples have an average grain size of 350, 500, 790 and 1000 nm (Table 2 and Fig. 2), respectively. This fact establishes the

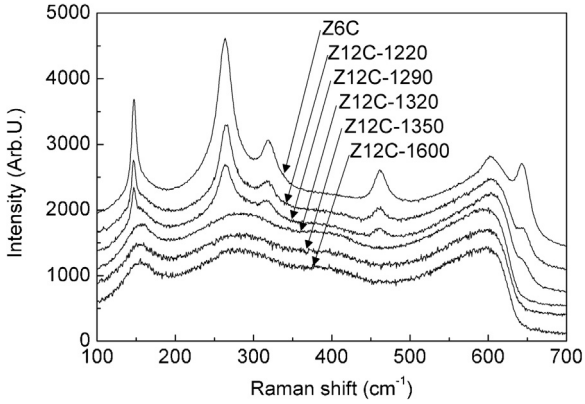

Fig. 5. Raman spectra for Z12C sample series dense pellets.

critical average grain size for the t''-form/cubic transition in dense Z12C ceramics between 500 and 790 nm. A similar analysis for the Z9Y series establishes this limit between 500 and 670 nm (Table 2 and Fig. 2).

It is worth mentioning that pure and doped zirconia powders tend to the high-temperature tetragonal/cubic structures with a decreasing crystallite size [21,22]. Shukla and Seal [20] shown that thermal treatments, with the consequent increase in crystallite size, transform powders to the thermodynamically stable monoclinic phase. This happens because in powders, the surface free energy is a determinant factor in the retention of high temperature phases [26] and becomes more important while crystallite size decreases [20].

In ceramics, the situation is different, the grains are large enough so the surface free energy effect is minimized or negligible, and as they are in intimate contact with each other the interfacial energy can have a significant role [20]. For example, for a highly agglomerated nanocrystalline ZrO_2 powder, in which the surface energies are modified and can be regarded as interfacial energies, it was found that the high temperature tetragonal phase is stable at room temperature up to a critical size of 30–33 nm [51]. Notice that this size decreases to 10 nm for strain free, single domain crystallites of near-spherical shape in contact with air at ambient pressure and temperature [52]. Al_2O_3-coated ZrO_2 nanoparticles exhibit an increase in both the tetragonal-to-monoclinic phase transformation temperature (1000 to 1400 °C) and the maximum critical domain-size for the tetragonal phase stabilization at room temperature (~20 to ~70 nm) [53].

Shukla and Seal [20], Garvie [51], Garvie and Goss [52], and Kirch and Tolbert [53] report about the monoclinic/tetragonal transition, a more dramatic change in crystal structure with a much larger volume change of ~4%, than the tetragonal/cubic one (~0.1% volume change) [48]. A similar mechanism, i.e., a modification of the interfacial energy of the grains, could explain the stabilization of the cubic phase in the larger grain ceramics studied in this work. However, the explanation of this phenomenon is outside the scope of this paper.

3.3. Bulk electrical properties

Further evidence for the presence of the tetragonal or cubic phases in the pellets can be obtained by calculating the activation energy (Ea) for bulk ionic conduction. EIS measurements were made for all samples. We used the Z6C and Z3Y and the Z12C-1600 and Z9Y-1600 pellets as phase standards. These samples are well characterized in dense ceramics and known to present the tetragonal or the cubic phase, respectively [34–36,43,44,54].

Please cite this article in press as: I.O. Fábregas, et al., Grain-size/(t'' or c)-phase relationship in dense ZrO_2 ceramics, *J Eur Ceram Soc* (2016), http://dx.doi.org/10.1016/j.jeurceramsoc.2016.01.048

We also conducted a literature survey of reported Ea's. All Ea's reported in Table 2 are from data taken below 500 °C, as is our data. Between 500 °C and 600 °C, the oxide ion vacancy dissociates from the dopant [55] and the Ea decreases. For lightly doped tetragonal samples, we can clearly see in Table 2 that the activation energy is lower than for more heavily cubic doped samples. This dependence of the Ea on composition can be rationalized if we consider that a molecular dynamics study found that the Ea increases with higher dopant content [56].

The Z8Y sample Ref. [41], presents an anomalously low Ea value. No ceramic D_g is reported, but with 4 h at 1650 °C as the sintering process is doubtful its D_g is below the t''/c boundary. In addition, the authors did not discuss its relevance, insofar as such a low Ea value is very remarkable for zirconia ionic conduction at low temperature. Specially, since these values are even lower than those accepted for tetragonal zirconia, and heavily doped samples have a higher Ea [56]. For these reasons, these samples were not considered any further. No D_g is reported for Refs. [43,44] samples, but with the sintering process utilized, the D_g is surely above the boundary determined here. The Z8Y samples from [23,42] are nanocristalline ceramics with a D_g smaller than 351 nm, below the t''/c boundary determined in this work. No structural characterization is reported, but, interestingly, they present very similar Ea values than those of our t''-samples.

Table 2 presents the bulk Ea for ionic conduction for all the samples studied here; it is clear that the Ea changes. Furthermore, this change matches perfectly with the change in crystal symmetry and cannot be assigned to an increase in density and/or grain size (reported in Table 2), as studies done in [23,24,39,42] showed that the Ea was independent of these factors. Although there is some dispersion in the Ea values reported in Table 2, there is no overlap between tetragonal and cubic samples. In addition, the majority of the cubic samples, presented an Ea value that was above the one determined in this work for t''-samples.

The lower Ea value for Z12C-1220, Z12C-1290, Z9Y-1220 and Z9Y-1250 is then closer to the accepted values for the tetragonal phase, than to those for the cubic one (see Table 2), suggesting that these samples did not present the cubic phase.

The change in the bulk ionic conduction Ea is further evidence, independently obtained, that supports the phase transition from the t'' form of the tetragonal phase to the cubic one for both series.

4. Conclusions

Monophasic ceramic pellets of different average grain size were obtained. A tendency for dense ceramics to stabilize the t'' phase for smaller grains, as opposed to the tendency for pure and doped ZrO_2 powders to stabilize the cubic/tetragonal phases for smaller crystallite sizes, was observed.

The bulk ionic conduction Ea depended not only on the nature of the aliovalent dopant, but also on the crystal structure, a fact which is not thoroughly discussed in the literature, probably due to the difficulty of distinguishing between the t'' and cubic structures in ZrO_2 based systems.

In this work, the simultaneous utilization of XRD, Raman and EIS was used to determine the crystal structure of Z12C and Z9Y ceramic pellets with different grain sizes. Complementary information obtained from each technique was extremely useful to clarify whether the pellets presented the t'' or cubic structure.

We report for the first time the critical grain size for the t''/cubic transition in ZrO_2–12 mol% CaO, between 500 and 790 nm, and ZrO_2–9 mol% Y_2O_3, between 500 and 670 nm, dense ceramics.

Acknowledgments

This work was supported by the projects PICT-2007-01152 and PICT-2005-38309 of the Agencia Nacional de Promoción Científica y Tecnológica and PIP 6559 from the Consejo Nacional de Investigaciones Científicas y Técnicas. IOF is grateful to the Fundación YPF for his doctoral fellowship. There was no involvement of the funding body in study-design or data interpretation.

References

[1] G.G.M. Fournier, I.W. Cumming, K. Hellgardt, High performance direct ammonia solid oxide fuel cell, J. Power Sources 162 (1) (2006) 198–206, http://dx.doi.org/10.1016/j.jpowsour.2006.06.047.
[2] M. Zhou, A. Ahmad, Processing and characterization of oxygen sensors prepared from freeze-dried calcia-stabilized zirconia powders, Int. J. Appl. Ceram. Technol. 3 (3) (2006) 218–224, http://dx.doi.org/10.1111/j.1744-7402.2006.02075.x.
[3] M. Zhou, A. Ahmad, Synthesis, processing and characterization of calcia-stabilized zirconia solid electrolytes for oxygen sensing applications, Mater. Res. Bull. 41 (4) (2006) 690–696, http://dx.doi.org/10.1016/j.materresbull.2005.10.018.
[4] Impedance Spectroscopy: Theory, Experiment, and Applications. 2005, Wiley-Interscience, Hoboken.
[5] R. Chiba, T. Ishii, F. Yoshimura, Temperature dependence of ionic conductivity in $(1-x)ZrO_2$–$(x-y)Sc_2O_3$–yYb_2O_3 electrolyte material, Solid State Ion. 91 (3–4) (1996) 249–256, http://dx.doi.org/10.1016/S0167-2738(96)83026-8.
[6] W. Huang, P. Shuk, M. Greenblatt, M. Croft, F. Chen, M. Liu, Structural and electrical characterization of a novel mixed conductor: CeO_2–Sm_2O_3–ZrO_2 solid solution, J. Electrochem. Soc. 147 (11) (2000) 4196–4202, http://dx.doi.org/10.1149/1.1394040.
[7] J. Drennan, G. Auchterlonie, Microstructural aspects of oxygen ion conduction in solids, Solid State Ion. 134 (1–2) (2000) 75–87, http://dx.doi.org/10.1016/S0167-2738(00)00716-5.
[8] N.Q. Minh, T. Takahashi, Preface, in: N.Q.M. Takahashi (Ed.), Science and Technology of Ceramic Fuel Cells, Elsevier Science Ltd., Oxford, 1995, pp. vii–viii.
[9] M. Yashima, M. Kakihana, M. Yoshimura, Metastable–stable phase diagrams in the zirconia-containing systems utilized in solid-oxide fuel cell application, Solid State Ion. 86–88 (Pt. 2) (1996) 1131–1149, http://dx.doi.org/10.1016/0167-2738(96)00386-4.
[10] R.E. Juarez, D.G. Lamas, G.E. Lascalea, N.E. Walsöe de Reca, Synthesis and structural properties of zirconia-based nanocrystalline powders and fine-grained ceramics, Defect Diffus. Forum 177–178 (1999) 1–28.
[11] D.G. Lamas, R.O. Fuentes, I.O. Fabregas, M.E. Fernandez de Rapp, G.E. Lascalea, J.R. Casanova, N.E. Walsoe de Reca, A.F. Craievich, Synchrotron X-ray diffraction study of the tetragonal-cubic phase boundary of nanocrystalline ZrO_2–CeO_2 synthesized by a gel-combustion process, J. Appl. Crystallogr. 38 (6) (2005) 867–873, http://dx.doi.org/10.1107/S0021889805025343.
[12] I.O. Fábregas, R.O. Fuentes, D.G. Lamas, M.E. Fernandez de Rapp, N.E. Walsoe de Reca, M.C.A. Fantini, A.F. Craievich, R.J. Prado, R.P. Millen, M.L.A. Temperini, Local structure of the metal–oxygen bond in compositionally homogeneous, nanocrystalline zirconia–ceria solid solutions synthesized by a gel-combustion process, J. Phys. Condens. Matter 18 (34) (2006) 7863.
[13] I.O. Fabregas, D.G. Lamas, N.E. Walsoe de Reca, M.C.A. Fantini, A.F. Craievich, R.J. Prado, Synchrotron X-ray powder diffraction and extended X-ray absorption fine structure spectroscopy studies on nanocrystalline ZrO_2–CaO solid solutions, J. Appl. Crystallogr. 41 (4) (2008) 680–689, http://dx.doi.org/10.1107/S0021889808013046.
[14] I.O. Fábregas, D.G. Lamas, L.M. Acuña, N.E. Walsöe de Reca, A.F. Craievich, M.C.A. Fantini, R.J. Prado, Crystal structure and local order of nanocrystalline zirconia-based solid solutions, Powder Diffr. 23 (Suppl. 1) (2008) S46–S55, http://dx.doi.org/10.1154/1.2903503.
[15] I.O. Fábregas, A.F. Craievich, M.C.A. Fantini, R.P. Millen, M.L.A. Temperini, D.G. Lamas, Tetragonal-cubic phase boundary in nanocrystalline ZrO_2–Y_2O_3 solid solutions synthesized by gel-combustion, J. Alloys Compd. 509 (16) (2011) 5177–5182, http://dx.doi.org/10.1016/j.jallcom.2011.01.213.
[16] M. Yashima, S. Sasaki, Y. Yamaguchi, M. Kakihana, M. Yoshimura, T. Mori, Internal distortion in ZrO_2–CeO_2 solid solutions: neutron and high-resolution synchrotron X-ray diffraction study, Appl. Phys. Lett. 72 (2) (1998) 182–184, http://dx.doi.org/10.1063/1.120678.
[17] O. Sahin, I. Demirkol, H. Göcmez, M. Tuncer, H.A. Cetinkara, H.S. Güder, E. Sahin, A.R. Tuncdemir, M.D. Cabezas, Mechanical properties of nano crystalline tetragonal zirconia stabilized with CaO, MgO and Y_2O_3, Acta Phys. Pol. A 123 (2) (2013) 300.
[18] M. Pakala, H. Walls, R.Y. Lin, Microhardness of sputter-deposited zirconia films on silicon wafers, J. Am. Ceram. Soc. 80 (6) (1997) 1477–1484, http://dx.doi.org/10.1111/j.1151-2916.1997.tb03006.x.
[19] B. Basu, Toughening of yttria-stabilised tetragonal zirconia ceramics, Int. Mater. Rev. 50 (4) (2005) 239–256, http://dx.doi.org/10.1179/174328005X41113.

Please cite this article in press as: I.O. Fábregas, et al., Grain-size/(t'' or c)-phase relationship in dense ZrO_2 ceramics, *J Eur Ceram Soc* (2016), http://dx.doi.org/10.1016/j.jeurceramsoc.2016.01.048

[20] S. Shukla, S. Seal, Mechanisms of room temperature metastable tetragonal phase stabilisation in zirconia, Int. Mater. Rev. 50 (1) (2005) 45–64, http://dx.doi.org/10.1179/174328005X14267.
[21] D.G. Lamas, A.M. Rosso, M.S. Anzorena, A. Fernández, M.G. Bellino, M.D. Cabezas, N.E. Walsöe de Reca, A.F. Craievich, Crystal structure of pure ZrO_2 nanopowders, Scr. Mater. 55 (6) (2006) 553–556, http://dx.doi.org/10.1016/j.scriptamat.2006.05.035.
[22] W. Yuren, L. Kunquan, W. Dazhi, W. Zhonghua, F. Zhengzhi, The EXAFS study of nanocrystalline zirconia, J. Phys. Condens. Matter 6 (3) (1994) 633.
[23] S. Boulfrad, E. Djurado, L. Dessemond, Blocking effect in high purity nanostructured cubic zirconia ceramics, Fuel Cells 8 (5) (2008) 313–321, http://dx.doi.org/10.1002/fuce.200800016.
[24] M. Aoki, Y.-M. Chiang, I. Kosacki, L.J.-R. Lee, H. Tuller, Y. Liu, Solute segregation and grain-boundary impedance in high-purity stabilized zirconia, J. Am. Ceram. Soc. 79 (5) (1996) 1169–1180, http://dx.doi.org/10.1111/j.1151-2916.1996.tb08569.x.
[25] I.O. Fabregas, Fases metaestables y nuevas propiedades en materiales nanoestructurados basados en ZrO_2. Aplicaciones en celdas de combustible de óxido sólido, in: PhD Dissertation, Universidad de Buenos Aires, Buenos Aires, Argentina, 2008 (in Spanish).
[26] I. Kosacki, T. Suzuki, V. Petrovsky, H.U. Anderson, Electrical conductivity of nanocrystalline ceria and zirconia thin films, Solid State Ion. 136–137 (2000) 1225–1233, http://dx.doi.org/10.1016/S0167-2738(00)00591-9.
[27] X. Guo, E. Vasco, S. Mi, K. Szot, E. Wachsman, R. Waser, Ionic conduction in zirconia films of nanometer thickness, Acta Mater. 53 (19) (2005) 5161–5166, http://dx.doi.org/10.1016/j.actamat.2005.07.033.
[28] I.O. Fábregas, D.G. Lamas, Parametric study of the gel-combustion synthesis of nanocrystalline ZrO_2-based powders, Powder Technol. 214 (2) (2011) 218–228, http://dx.doi.org/10.1016/j.powtec.2011.08.013.
[29] A.C. Larson, R.B.V. Dreele, General Structure Analysis System (GSAS), Los Alamos National Laboratory Report, Los Alamos, 2000230.
[30] B.H. Toby, EXPGUI, a graphical user interface for GSAS, J. Appl. Crystallogr. 34 (2) (2001) 210–213, http://dx.doi.org/10.1107/s0021889801002242.
[31] N.P. Louat, On the theory of normal grain growth, Acta Metall. 22 (6) (1974) 721–724, http://dx.doi.org/10.1016/0001-6160(74)90081-9.
[32] M.P. Anderson, G.S. Grest, D.J. Srolovitz, Computer simulation of normal grain growth in three dimensions, Philos. Mag. Part B 59 (3) (1989) 293–329, http://dx.doi.org/10.1080/13642818908220181.
[33] M. Elsey, S. Esedoglu, P. Smereka, Large-scale simulation of normal grain growth via diffusion-generated motion, Proc. R. Soc. Lond. A (2010) 1–21, http://dx.doi.org/10.1098/rspa.2010.0194.
[34] G. Bernard-Granger, C. Guizard, S. Surblé, G. Baldinozzi, A. Addad, Spark plasma sintering of a commercially available granulated zirconia powder—II. Microstructure after sintering and ionic conductivity, Acta Mater. 56 (17) (2008) 4658–4672, http://dx.doi.org/10.1016/j.actamat.2008.05.031.
[35] P. Mondal, A. Klein, W. Jaegermann, H. Hahn, Enhanced specific grain boundary conductivity in nanocrystalline Y_2O_3-stabilized zirconia, Solid State Ion. 118 (3–4) (1999) 331–339, http://dx.doi.org/10.1016/S0167-2738(98)00452-4.
[36] B.A. Boukamp, T.P. Raming, A.J.A. Winnubst, H. Verweij, Electrochemical characterisation of 3Y-TZP–Fe_2O_3 composites, Solid State Ion. 158 (3–4) (2003) 381–394, http://dx.doi.org/10.1016/S0167-2738(02)00841-X.
[37] M. Weller, H. Schubert, Internal friction, dielectric loss, and ionic conductivity of tetragonal ZrO_2–3% Y_2O_3 (Y-TZP), J. Am. Ceram. Soc. 69 (7) (1986) 573–577, http://dx.doi.org/10.1111/j.1151-2916.1986.tb04795.x.
[38] F.T. Ciacchi, K.M. Crane, S.P.S. Badwal, Evaluation of commercial zirconia powders forsolid oxide fuel cells, Solid State Ion. 73 (1–2) (1994) 49–61, http://dx.doi.org/10.1016/0167-2738(94)90263-1.
[39] X. Guo, Z. Zhang, Grain size dependent grain boundary defect structure: case of doped zirconia, Acta Mater. 51 (9) (2003) 2539–2547, http://dx.doi.org/10.1016/S1359-6454(03)00052-1.
[40] X. Guo, J. Maier, Grain boundary blocking effect in zirconia: a Schottky barrier analysis, J. Electrochem. Soc. 148 (3) (2001) E121–E126, http://dx.doi.org/10.1149/1.1348267.
[41] J. Gong, Y. Li, Z. Zhang, Z. Tang, ac impedance study of zirconia doped with yttria and calcia, J. Am. Ceram. Soc. 83 (3) (2000) 648–650, http://dx.doi.org/10.1111/j.1151-2916.2000.tb01247.x.
[42] N.H. Perry, S. Kim, T.O. Mason, Local electrical and dielectric properties of nanocrystalline yttria-stabilized zirconia, J. Mater. Sci. 43 (14) (2008) 4684–4692, http://dx.doi.org/10.1007/s10853-008-2553-x.
[43] M. Bučko, Some structural aspects of ionic conductivity in zirconia stabilised by yttria and calcia, Mater. Sci. Pol. 24 (1) (2006) 39–44.
[44] A.J. Feighery, J.T.S. Irvine, Effect of alumina additions upon electrical properties of 8 mol% yttria-stabilised zirconia, Solid State Ion. 121 (1–4) (1999) 209–216, http://dx.doi.org/10.1016/S0167-2738(99)00015-6.
[45] C. Chen, H. Wang, J. Ji, M. Luo, B. Wu, M. Hu, H. Xia, Z. Huang, Preparation and electrical property of calcia stabilized zirconia ceramics, Key Eng. Mater. 616 (2014) 157–165, http://dx.doi.org/10.4028/www.scientific.net/KEM.616.157.
[46] S.H. Chu, M.A. Seitz, The ac electrical behavior of polycrystalline ZrO_2–CaO, J. Solid State Chem. 23 (3–4) (1978) 297–314, http://dx.doi.org/10.1016/0022-4596(78)90078-6.
[47] M. Yashima, In situ observations of phase transition using high-temperature neutron and synchrotron X-ray powder diffractometry, J. Am. Ceram. Soc. 85 (12) (2002) 2925–2930, http://dx.doi.org/10.1111/j.1151-2916.2002.tb00557.x.
[48] J.A. Krogstad, M. Lepple, Y. Gao, D.M. Lipkin, C.G. Levi, Effect of yttria content on the zirconia unit cell parameters, J. Am. Ceram. Soc. 94 (12) (2011) 4548–4555, http://dx.doi.org/10.1111/j.1551-2916.2011.04862.x.
[49] M. Yashima, M. Kakihana, K. Ishii, Y. Ikuma, M. Yoshimura, Synthesis of metastable tetragonal (t') zirconia–calcia solid solution by pyrolysis of organic precursors and coprecipitation route, J. Mater. Res. 11 (6) (1996) 1410–1420, http://dx.doi.org/10.1557/JMR.1996.0177.
[50] M. Yashima, K. Ohtake, H. Arashi, M. Kakihana, M. Yoshimura, Determination of cubic-tetragonal phase boundary in $Zr_{1-x}Y_xO_{2-x/2}$ solid solutions by Raman spectroscopy, J. Appl. Phys. 74 (12) (1993) 7603–7605, http://dx.doi.org/10.1063/1.354989.
[51] R.C. Garvie, The occurrence of metastable tetragonal zirconia as a crystallite size effect, J. Phys. Chem. 69 (4) (1965) 1238–1243, http://dx.doi.org/10.1021/j100888a024.
[52] R.C. Garvie, M.F. Goss, Intrinsic size dependence of the phase transformation temperature in zirconia microcrystals, J. Mater. Sci. 21 (4) (1986) 1253–1257, http://dx.doi.org/10.1007/bf00553259.
[53] B.L. Kirsch, S.H. Tolbert, Stabilization of isolated hydrous amorphous and tetragonal zirconia nanoparticles through the formation of a passivating alumina shell, Adv. Funct. Mater. 13 (4) (2003) 281–288, http://dx.doi.org/10.1002/adfm.200304267.
[54] A. Brune, M. Lajavardi, D. Fisler, J.B. Wagner Jr., The electrical conductivity of yttria-stabilized zirconia prepared by precipitation from inorganic aqueous solutions, Solid State Ion. 106 (1–2) (1998) 89–101, http://dx.doi.org/10.1016/S0167-2738(97)00486-4.
[55] Y. Arachi, H. Sakai, O. Yamamoto, Y. Takeda, N. Imanishai, Electrical conductivity of the ZrO_2–Ln_2O_3 (Ln = lanthanides) system, Solid State Ion. 121 (1–4) (1999) 133–139, http://dx.doi.org/10.1016/S0167-2738(98)00540-2.
[56] Y. Yamamura, S. Kawasaki, H. Sakai, Molecular dynamics analysis of ionic conduction mechanism in yttria-stabilized zirconia, Solid State Ion. 126 (1–2) (1999) 181–189, http://dx.doi.org/10.1016/S0167-2738(99)00227-1.

Please cite this article in press as: I.O. Fábregas, et al., Grain-size/(t'' or c)-phase relationship in dense ZrO_2 ceramics, *J Eur Ceram Soc* (2016), http://dx.doi.org/10.1016/j.jeurceramsoc.2016.01.048